materials

MDPI

Article

A Novel P@SiO_2 Nano-Composite as Effective Adsorbent to Remove Methylene Blue Dye from Aqueous Media

AbdElAziz A. Nayl [1,*], Ahmed I. Abd-Elhamid [2], Wael A. A. Arafa [1], Ismail M. Ahmed [1], Aref M. E. AbdEl-Rahman [2], Hesham M. A. Soliman [2], Mohamed A. Abdelgawad [3], Hazim M. Ali [1], Ashraf A. Aly [4] and Stefan Bräse [5,6,*]

1 Department of Chemistry, College of Science, Jouf University, Sakaka 72341, Aljouf, Saudi Arabia
2 Composites and Nanostructured Materials Research Department, Advanced Technology and New Materials Research Institute, City of Scientific Research and Technological Applications (SRTA-City), New Borg Al-Arab 21934, Egypt
3 Department of Pharmaceutical Chemistry, College of Pharmacy, Jouf University, Sakaka 72341, Aljouf, Saudi Arabia
4 Chemistry Department, Faculty of Science, Organic Division, Minia University, El-Minia 61519, Egypt
5 Institute of Organic Chemistry (IOC), Karlsruhe Institute of Technology (KIT), Fritz-Haber-Weg 6, 76133 Karlsruhe, Germany
6 Institute of Biological and Chemical Systems-Functional Molecular Systems (IBCS-FMS), Hermann-von-Helmholtz-Platz 1, 76344 Eggenstein-Leopoldshafen, Germany
* Correspondence: aanayel@ju.edu.sa (A.A.N.); stefan.braese@kit.edu (S.B.)

Abstract: This work aims to prepare a novel phosphate-embedded silica nanoparticles (P@SiO_2) nanocomposite as an effective adsorbent through a hydrothermal route. Firstly, a mixed solution of sodium silicate and sodium phosphate was passed through a strong acidic resin to convert it into hydrogen form. After that, the resultant solution was hydrothermally treated to yield P@SiO_2 nanocomposite. Using kinetic studies, methylene blue (MB) dye was selected to study the removal behavior of the P@SiO_2 nanocomposite. The obtained composite was characterized using several advanced techniques. The experimental results showed rapid kinetic adsorption where the equilibrium was reached within 100 s, and the pseudo-second-order fitted well with experimental data. Moreover, according to Langmuir, one gram of P@SiO_2 nanocomposite can remove 76.92 mg of the methylene blue dye. The thermodynamic studies showed that the adsorption process was spontaneous, exothermic, and ordered at the solid/solution interface. Finally, the results indicated that the presence of NaCl did not impact the adsorption behavior of MB dye. Due to the significant efficiency and promising properties of the prepared P@SiO_2 nanocomposite, it could be used as an effective adsorbent material to remove various cationic forms of pollutants from aqueous solutions in future works.

Keywords: nanocomposite; adsorption; eco-friendly; methylene blue; wastewater

check for updates

Citation: Nayl, A.A.; Abd-Elhamid, A.I.; Arafa, W.A.A.; Ahmed, I.M.; AbdEl-Rahman, A.M.E.; Soliman, H.M.A.; Abdelgawad, M.A.; Ali, H.M.; Aly, A.A.; Bräse, S. A Novel P@SiO_2 Nano-Composite as Effective Adsorbent to Remove Methylene Blue Dye from Aqueous Media. *Materials* **2023**, *16*, 514. https://doi.org/10.3390/ma16020514

Academic Editors: Wen-Tien Tsai and Maria Harja

Received: 1 December 2022
Revised: 23 December 2022
Accepted: 28 December 2022
Published: 5 January 2023

Copyright: © 2023 by the authors. Licensee MDPI, Basel, Switzerland. This article is an open access article distributed under the terms and conditions of the Creative Commons Attribution (CC BY) license (https://creativecommons.org/licenses/by/4.0/).

1. Introduction

Many hazardous materials, such as heavy metals, dyes, drugs, pesticides, etc., have been discharged into the aquatic environment. This water pollution has become a severe universal subject and attracts attention worldwide from researchers, politicians, and simple people. Dyes are one of the more industrial effluents and are heavily used in several industries, such as food, wood, leather, paper, silk, etc. Discharging dyes in the aquatic sphere, even at low concentrations, will harm all living organisms that live in water, animals, and humans, where it is a toxic, carcinogenic, mutagenic, and non-degradable materials that can stay in the environment for a long time [1]. Methylene blue (MB) dye is the most famous water contaminant that badly impacts health through abdominal disorders, respiratory distress, skin sensitization, and blindness [2–4]. Also, methylene blue, with its

deep blue color, reduces the penetration of the light for aquatic organisms, which has a bad effect on the environment and disorders the balance of the ecosystem leading to dangerous issues for all forms of living systems and thus threatens their life [1,5–7]. Therefore, it is very important to decontaminate this dye from water to prevent its discharge into the environment, especially aquatic bio-systems [1]. So, the remediation of such pollutants has extraordinary value due to the water shortage that many countries face.

Several strategies have been investigated and developed to purify water from such harmful material, including photocatalytic degradation, solvent extraction, coagulation, biodegradation, oxidation, zonation, and adsorption [5,8,9]. Adsorption, among the techniques, is the most powerful, economical, and efficient technique utilized to decontaminate dyes from wastewater at low concentrations due to its simplicity, low cost, and not requiring advanced technology [10–13]. During this year, novel adsorbent materials have been reported to remove toxic dyes such as methylene blue from wastewater [14–27]. Activated carbon (AC) is one of the most traditional, effective, and extensively utilized adsorbents in adsorption technologies, and it is among the cheapest sorbents in market. However, its failure to regenerate is still considered a major setback [28], and recycling its powdered form from the liquid phase is another intractable issue [29]. Also, some investigated materials' main shortcomings cause them to be considered undesirable adsorbent materials due to their relatively higher cost and generation of secondary contaminants. Therefore, selecting proper adsorbent materials that produce low secondary contaminants with favorable chemical and thermal stability as well as suitable regeneration operations is the key to adsorption technologies [13]. So, scientists direct their works to investigate other alternative natural materials to treat the colored dyestuff effluents to overcome such disadvantages [30]. Siliceous adsorbents, such as silica, perlite, and glass fibers, are cost-effective and found naturally with good biocompatibility, excellent performance with non-toxicity, and considerable thermal stability in various applications, such as separation [31]. Due to the lower toxicity, easy availability, eco-friendly synthesis processes, cost-effectiveness, and bioactivity of SiO_2-NPs, it is safely used in food industries, drug delivery, pharmaceutical, and water treatment systems [9,32]. Also, it has higher efficiency in removing dyes such as MB dye, where silica nanoparticle adsorbents are characterized by high surface area, low toxicity, high stability, and economical preparation that enable them to serve as an efficient adsorbent in the water treatment processes. To enhance the removal capacities of such silica nanoparticles, the surface of the material has been modified by other materials [32]. Therefore, several processes were applied to surface silica particles for water treatments [33], especially in dye removal. The first is a reduction in particle size to nanoscale to obtain a great specific surface area [33]. Surface silica nanoparticles are also hybridized, functionalized, magnetized, and doped with polymers [33,34]. One or more of these processes is carried out to increase the adsorption capacity [34]. The presence of surface (-OH) groups attached to the Si-atom on SiO_2NPs is a very important characteristic and are termed silanols [34]. These silanols can interact selectively with dyes and are improved by changing the pH values [34]. Recently, many works have reported a great achievement for the new generation of silica-based nanomaterials, which illustrates outstanding adsorption capacities for several dyes by synthesis, functionalized, and hybrid SiO_2NPs [34]. Modifying the silica nanoparticles' surface will improve the adsorption performance [35]. Also reported in the literature, the surface of the silica nanoparticles was modified with organic chains involved in silane compounds. Jesionowski and Krysztafkiewicz [36] precipitated silica nanoparticles in an acidic solution followed by coupling with hydrophobic/hydrophilic function groups. Lee and Jo [**37**] prepared silica nanoparticles using the Stöber method and functionalized them with methyltriethoxysilane. Hah and Koo [**38**] synthesized silica nanoparticles using tetraethyl orthosilicate (TEOS) under a basic environment, and then methyltrimethoxysilane (MTMS) and vinyltrimethoxysilane (VTMS) were employed for anchoring the surface of the nanoparticles.

In previous studies, the modification of the silica nanoparticles was prepared through discontinuous processes with different steps and required expensive chemicals. Therefore,

in our present study, tri-sodium phosphate (Na_3PO_4), an inexpensive and valuable material, was grafted into silica nanoparticles through a simple and green hydrothermal route. Trisodium phosphate and sodium silicate were dissolved in an aqueous solution, passed through highly acidic resin, and finally, hydrothermally treated to produce a white precipitate (P@SiO_2 nanocomposite) which will be used as an effective adsorbent to the methylene blue (MB). The characterization of the fabricated P@SiO_2 nanocomposite was obtained with various physicochemical techniques such as scanning electron microscopy (SEM), X-ray diffraction analysis (XRD), elemental dispersive energy (EDX), and Fourier-transform infrared spectroscopy (FTIR). Also, the influences of the adsorption conditions, including P@SiO_2 nanocomposite dosage, initial MB dye concentrations, and solution pH, on the removal efficiencies were investigated. Also, the thermodynamic, kinetic and regeneration properties were studied.

2. Materials and Methods

2.1. Materials

Di-sodium silicate (Na_2SiO_3, Sigma-Aldrich, St. Louis, MO, USA), tri-sodium phosphate ($Na_3PO_4 \cdot 12H_2O$, 96%, Sigma-Aldrich), strong acid type of cation exchange resin (Rohm and Haas, Valbonne, France) and methylene blue (Sigma-Aldrich), NaCl (Sigma-Aldrich) were used.

2.2. Characterization and Analysis

The surface morphologies of the nanocomposite were detected using a scanning electron microscope (SEM, JEOL GSM-6610LV. Japan) operating at an acceleration voltage of 20 kV. The surfaces of the specimen were treated with a thin layer of gold before imaging. The dimension of the nanomaterial was measured using Image J software (Copyright 1998-2003 JEOL LDT) from the SEM captures in an original magnification of 30,000× and 50,000×. At least 25 isolated nanoparticles were randomly selected, and their diameters and diameter distributions were measured and averaged. The elemental analysis of the materials before and after the adsorption process was determined by the EDS unit connected with the SEM. The infrared spectrum of the nanoparticles was investigated by Fourier transform infrared spectrometer (FTIR, Shimadzu FTIR-8400 S, Japan) FTIR spectra. The infrared spectra were recorded in the transmission mode using nanomaterials mixed with KBr. The experiments were investigated in the range of 4000–400 cm^{-1}. The crystal structure of the composite was described by X-ray diffraction (XRD, Shimadzu, Japan XRD-7000) with a scanning speed of 12° min^{-1} from 5 to 100°.

2.3. Preparation of P@SiO_2 Nanocomposite

In a typical experiment, 9.0 g of di-sodium silicate and 2.0 g of tri-sodium phosphate were dissolved in 50 mL of double distilled water. After that, the previously prepared solution was loaded on a strong acid type of cation exchange resin column. The acidified solution was recovered from the column by elution. The eluted solution was charged into stainless steel autoclave reactor and placed in a muffle at 150 °C for 24 h. The resulting white powder centrifuge was washed several times with double distilled water and dried at 70 °C for 24 h. Figure S1 (in Supplementary Materials) shows the schematic diagram of the prepared powder.

2.4. Adsorption Studies

A methylene blue (MB) dye stock solution was investigated by stirring 1.0 g of the solid dye in 1.0 L of double distilled water, and the required concentrations were obtained by dilution. Batch removal experiments were prepared by stirring 10–25 mg of nanopowder (NPs) with 10 mL aqueous solution of methylene blue in 50 mL flasks at different concentrations (100–300 mg/L), pH (1.5–11), temperatures (25–80 °C), sodium chloride dose (0–2 g) and adsorbent tests take place at constant stirring speed. The nanopowder was isolated from the MB dye solution by centrifugation. The dye concentration residue

was analyzed using UV–vis spectroscopy at λ = 664 nm. The dye removal percent, %R, can be measured by applying the Equation (1):

$$\%R = \frac{C_o - C_e}{C_o} \times 100 \quad (1)$$

where C_o and C_e are the initial and equilibrium concentrations of the liquid phase of the dye (mg/L), respectively.

2.5. Mathematical Modeling

Adsorption kinetic, isotherm, and thermodynamic models investigated in our study are explained in the Supplementary Material file (Sections S1.1–S1.3, respectively).

3. Results and Discussion

3.1. Characterizations

Scanning electron microscopy (SEM) was applied to study the surface morphologies of the prepared P@SiO_2 nanocomposite. The SEM images of typical phosphate-doped silica (Si-P) nanoparticles are shown in Figure S1a–d. The prepared nanoparticles are spherical and have a diameter range (85–173 nm). The dimensions of the P@SiO_2 nanoparticles were determined using image J software from the SEM captures in an original magnification of 30,000× and 50,000×. The average diameters and diameter distributions for 25 randomly selected isolated nanoparticles were measured and averaged, as represented in Figure 1. The data obtained showed that the morphologies of the synthesized P@SiO_2 nanocomposite are relatively homogenous.

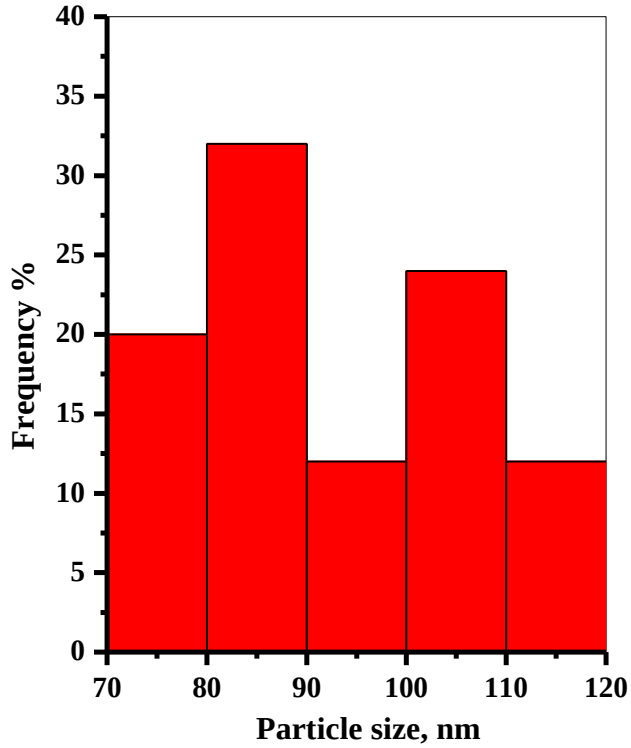


Figure 1. Histogram for the particle size distributions of the prepared P@SiO_2-nanoparticles.

FTIR spectra of silica and P@SiO_2 nanocomposite were investigated to obtain the basic information that illustrates the chemical structures of the prepared adsorbent material, as shown in Figure 2a.

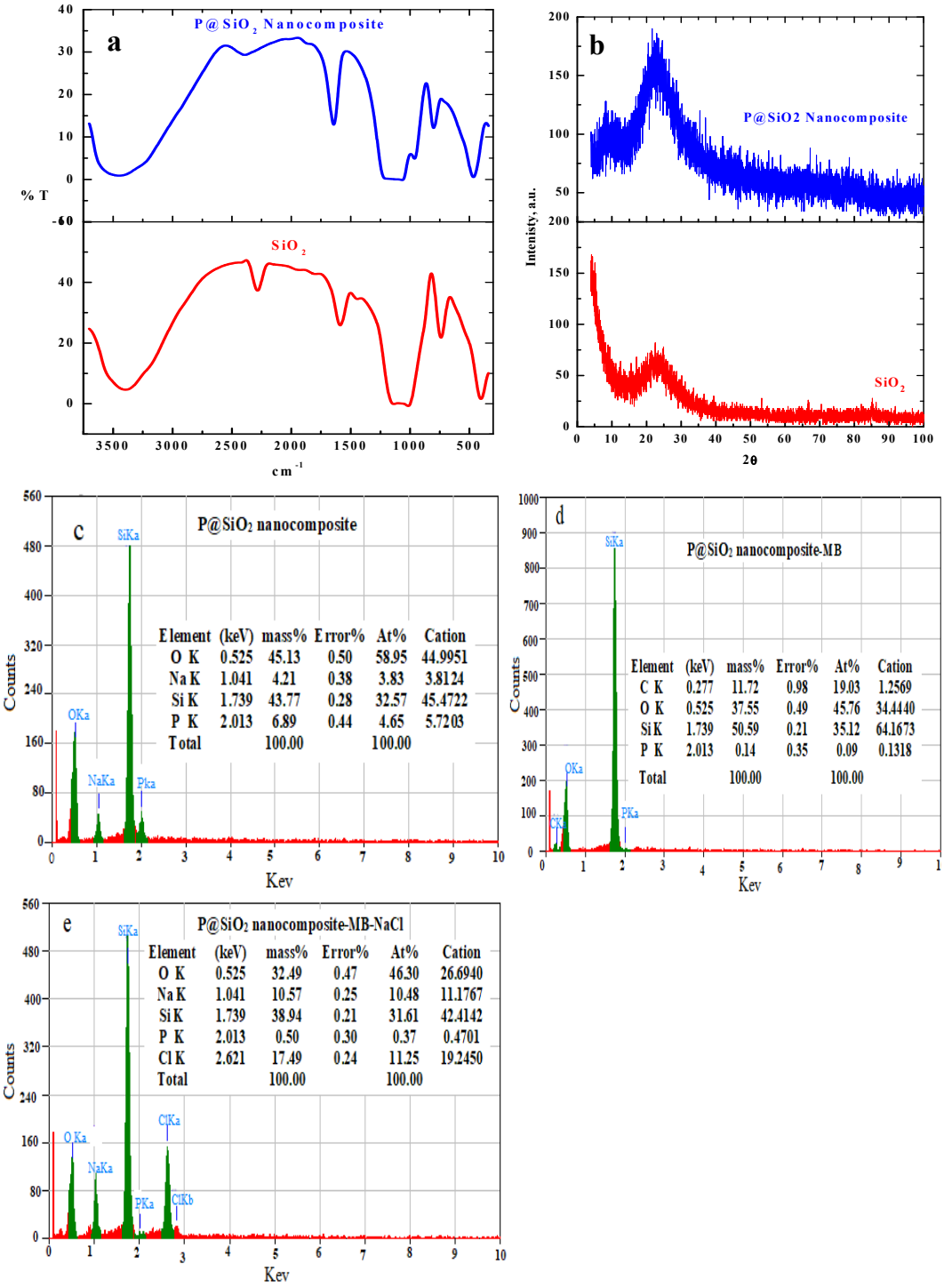


Figure 2. (**a**) FTIR spectrum of SiO_2 and P@SiO_2 nanoparticles, (**b**) XRD pattern of SiO_2 and P@SiO_2 nanoparticles, and EDS analysis of (**c**) Si-P and (**d**) P@SiO_2-MB and (**e**) P@SiO_2-MB-NaCl powder.

The common bands assigned to various vibrations of SiO_2 were observed. A broad band centered at around 3401 cm^{-1} corresponds to the stretching bands of the H-bonded H_2O molecules in the interlayer [35]. The adsorbed water molecules show a bending vibrations band at 1597 cm^{-1} [35]. Two strong bands appear at 1016 cm^{-1} and 1136 cm^{-1} corresponding to the Si-O-Si asymmetric stretching vibrations [33]. Furthermore, the symmetric stretching and the bending mode vibrations of Si-O-Si appear at 738 cm^{-1} [39] and 405 cm^{-1}, respectively. Upon addition of phosphate to form Si-P, these peaks have a

shift (405→467, 738→800, 1016→1066, 1136→1226, 1597→1646, and 3401→3465) [40]. A strong band at 1066 and 956 cm^{-1}, a characteristic of a $PO_4{}^{-3}$ group, was detected [41]. All of these mentioned spectral data prove that the P@SiO_2 nanocomposite was successfully prepared and has many active groups on the prepared P@SiO_2 nanocomposite surface that enhance the adsorption processes.

X-ray diffraction patterns were investigated to obtain information about the internal structures of SiO_2 and P@SiO_2 nanocomposites. The data obtained showed a broad peak at $2\theta \approx 20^\circ$ and broad peaks due to the amorphous nature of the synthesized P@SiO_2 nanocomposite, as represented in Figure 2b [42]. Also, other diffraction peaks were not observed at 2θ = 0.5–10°, due to the exchanges of hydrated protons and cations between the interlayers [35].

EDS measurements of P@SiO_2 nanocomposite (Figure 2c), P@SiO_2-MB (Figure 2d), and P@SiO_2-MB (Figure 2e) in the presence of NaCl (P@SiO_2-MB-NaCl) are presented in Figure 2c. The diagram shows that the prepared P@SiO_2 powder consists of Si, O, P, and Na, as demonstrated in Figure 2c. After interaction with the MB dye, the introduction of C is detected in the analyzed powder (P@SiO_2-MB) (as illustrated in Figure 2c). Moreover, to evaluate the influence of ionic strength on the adsorption of MB dye onto P@SiO_2 nanocomposite, the elements of Na and Cl were observed in the powder (P@SiO_2-MB-NaCl). This result proves that NaCl does not has any influence on the adsorption process under the investigated conditions

3.2. Adsorption Study

3.2.1. Effect of Contact Time and P@SiO_2 Nanocomposite Dose

The effect of contact time on the adsorption percentage (%R) of MB dye was tested using various P@SiO_2 nanocomposite adsorbents mixed with a defined concentration of MB dye (10–25 mg/10 mL) at a period of 0.0–400 s. The removal percentages (%R) of the MB dye increased linearly with the time increase to 100 s (Figure 3a). This is an attractive property of the promising P@SiO_2 nanocomposite and gives it added value to use as an effective and economical adsorbent material in wastewater treatment processes.

To study the effect of the P@SiO_2 nanocomposite dose on the uptake of the MB dye species, various weights of P@SiO_2 (10–25 mg/10 mL) were tested at constant other conditions ([MB] = 100 ppm, pH = 7, and T = 25 °C), as shown in Figure 3b. Also, it can be observed that the (%R) increased from 80.2 to 94.8%, with a further increase in the adsorbent dose from 10 to 25 mg, as illustrated in Figure 3b. This is attributed to increasing the number of active sites with an increase in the adsorbent dose, which enhances the removal percentage of MB dye molecules [43]. On the other hand, the increase in the adsorbent dose leads to a reduction in the amount of dye adsorbed to one gram of the adsorbent; this causes a decrease in q_e value as the adsorbent dose increase [43], as shown in Figure 3b. Figure S2 represented the relation between q_e vs. C_e at different (a) P@SiO_2 nanocomposite doses and (b) initial MB concentrations.

3.2.2. Effect of Initial MB Dye Concentration

The effect of the initial MB dye concentrations on the removal percent (%R) and the equilibrium adsorption amount of the MB dye by P@SiO_2 nanocomposite from an aqueous solution was investigated (as in Figure 3c) using initial MB dye concentrations ranging from 100 to 300 mg L^{-1} at adsorbent dose = 25 mg/10 mL, pH = 7, and T = 25 °C. It was observed that the %R increased with the time of the initial concentration to 100 s. After that, the equilibrium state was reached, as shown in Figure 2c. Moreover, the adsorption capacity of MB dye (q_e) increases with a further increase in the initial dye concentration in the range (100–300 mg L^{-1}), as presented in Figure 3d. The reason for this may refer to the increase in the MB dye concentrations causing improvement in the concentration gradient's driving force, which accelerates the MB dye species' diffusion velocity into the P@SiO_2 nanocomposite adsorbent particles [44]. Then, the concentration gradient reduces due to the adsorption of MB molecules on the active sites of the P@SiO_2 nanocomposite.

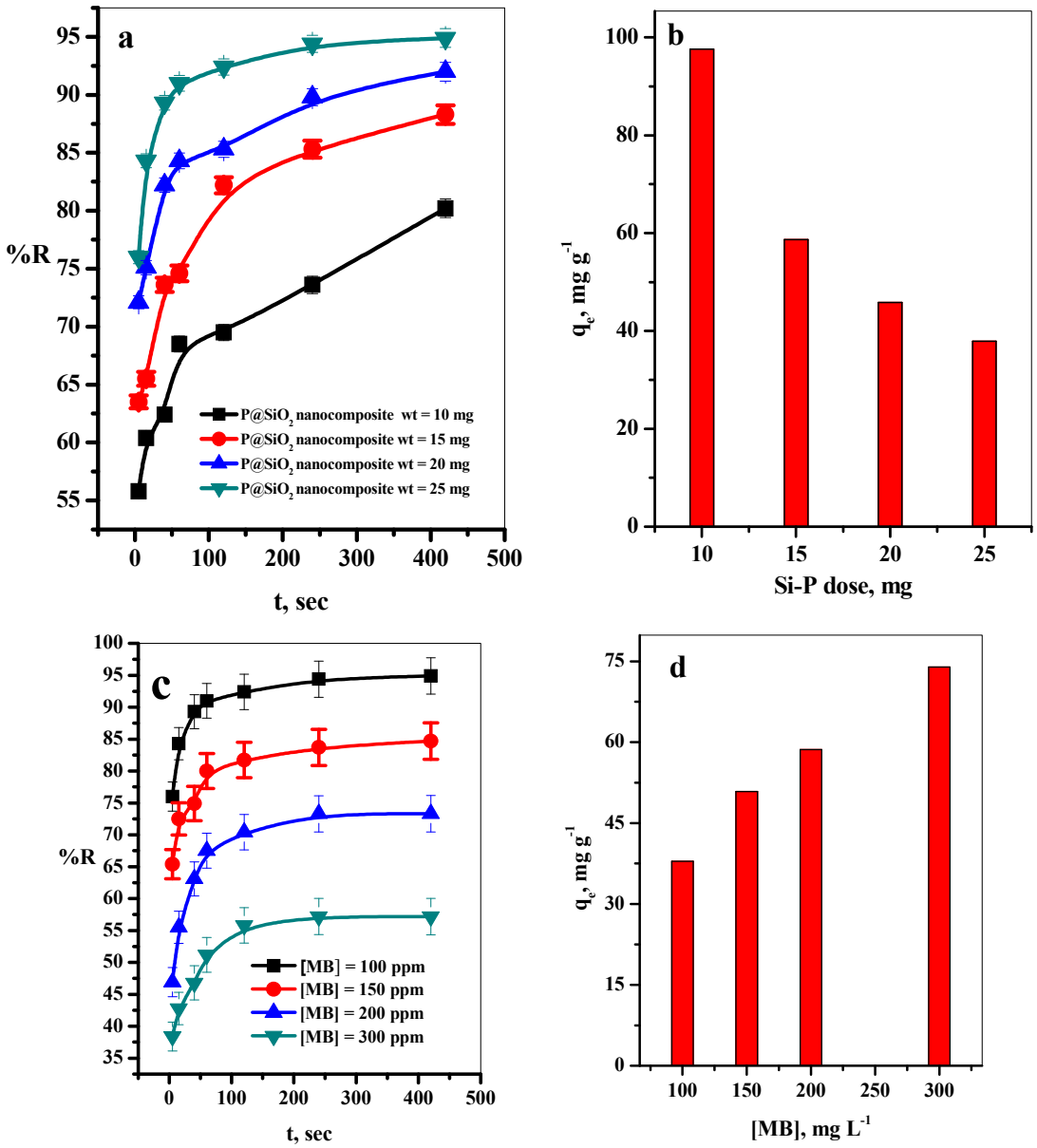


Figure 3. Effect of (**a**) P@SiO_2 nanocomposite doses at the different contact times, (**b**) effect of P@SiO_2 nanocomposite doses on q_e values, (**c**) effect of initial MB concentrations at the different contact time, and (**d**) its effect on q_e values, on the adsorption of MB dye. (P@SiO_2 dose ([MB] = 100 mg/L/10 mL, pH = 7, T = 25 °C) and (**d**) initial MB concentrations ([P@SiO_2] = 25 mg/10 mL, pH = 7, T = 25 °C).

In other words, at higher initial concentrations of MB, the binding sites of P@SiO_2 nanocomposite adsorbent were encompassed with many MB species in the solution. Hence, the adsorption capacity of the P@SiO_2 nanocomposite was enhanced by increasing the MB concentration, enhancing the adsorption capacity [45].

3.2.3. Effect of pH

The pH of the aqueous media is a very important factor in the adsorption process. The pH value affects the surface charge of the P@SiO_2 nanocomposite adsorbent and the degree of the ionization of the MB dye species. The effect of the pH was studied in the range 1.5–11 (by adjusting the pH with HCl (0.1 N) and NaOH (0.1 N) solutions) ([MB dye] = 150 ppm, [P@SiO_2 nanocomposite] = 25 mg/10 mL, T = 25 °C) on the removal percent %R of the MB dye by P@SiO_2 nanocomposite was performed in Figure 4a. It was observed that the removal percentages were changed with further variation in the pH values as the following;

at pH = 1.5, 3.0, 7.0, 9.0, and 11.0 the %R was 96.6, 67.1, 84.7, 99.7, and 95.3%, respectively. Consequently, the maximum adsorption capacities varied according to the pH values, as shown in Figure 4b.

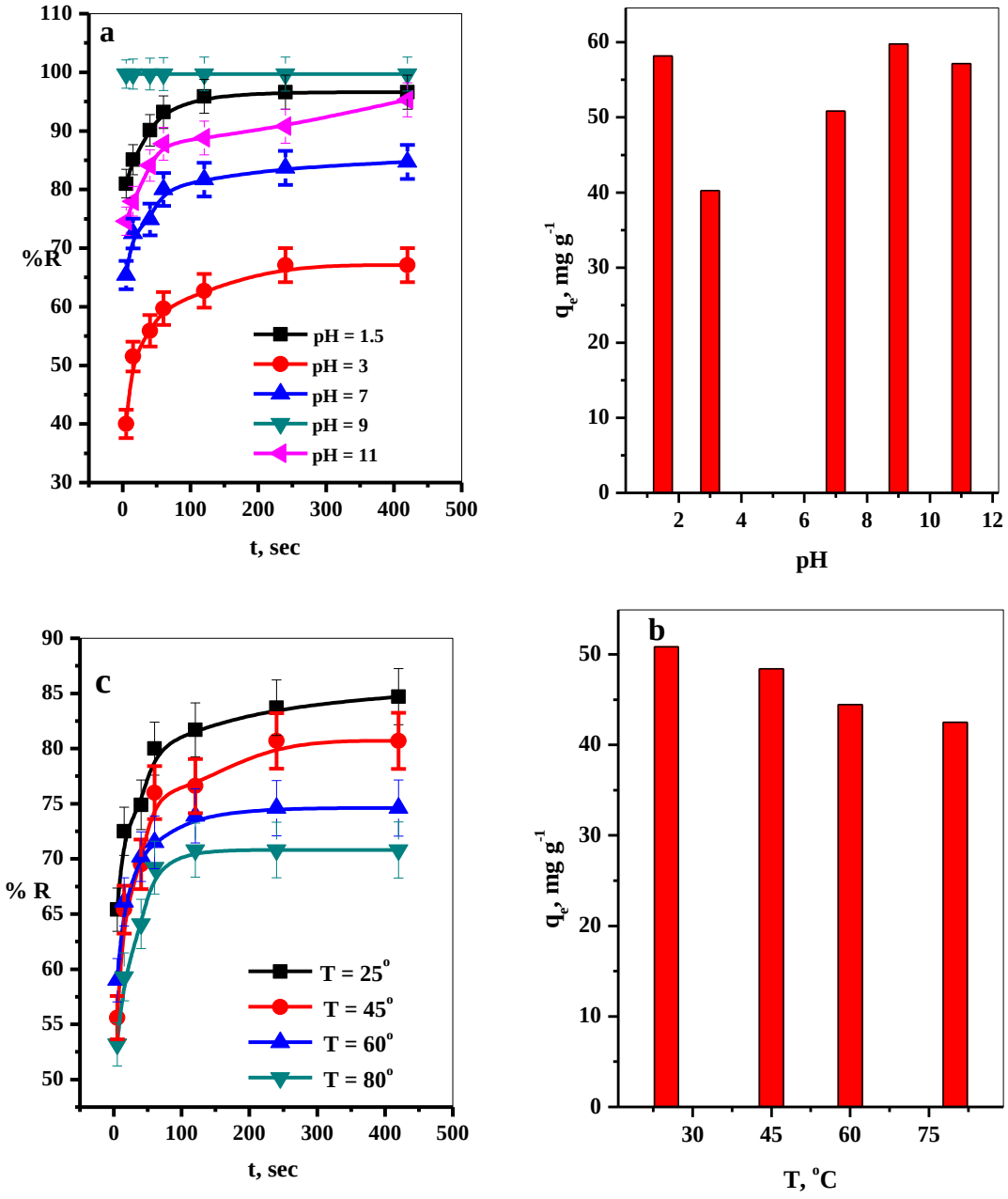


Figure 4. Effect of (**a**) pH, (**b**) effect of pH on q_e values, (**c**) effect of temperature, and (**d**) its effect on q_e values, on the adsorption of MB dye at different contact times ([P@SiO_2] = 25 mg, [MB] = 150 mg/L/10 mL, T = 25 °C) and (**d**) temperature ([P@SiO_2] = 25 mg, [MB] = 150 mg/L/10 mL, pH = 7).

Therefore, with an increase in the pH value of 3–9, the active groups on the P@SiO_2 nanocomposite are deprotonated to carry negative charges, leading to electrostatic interactions with MB molecules increasing the removal percentages. At pH > 9, the removal percentage decreased, and this may be attributed to the –OH-anions of NaOH which can inhibit the electrostatic interactions between P@SiO2 nanocomposite and MB molecules by blocking the positive charges on MB molecules surfaces [46].

The color intensity of the MB dye sample varied according to pH value and is represented in Figure S3.

3.2.4. Effect of Temperature

The influence of the temperature, ranged from 25 to 80 °C, on the %R of the MB dye from aqueous media onto P@SiO_2 nanocomposite at pH = 7, [MB] = 150 ppm, [P@SiO_2 nanocomposite] = 25 mg/10 mL was investigated and is represented in Figure 4c. It was found that the %R of the MB dye increased with the time the temperature degrees were used overall. Consequently, the removal percentages decreased as the temperature increased, as illustrated in Figure 4c. Furthermore, as the dye solution temperature rose, the adsorbate's maximum adsorption capacity decreased [47], as plotted in Figure 4d. This can be attributed to the exothermic nature of the adsorption process.

3.2.5. Adsorption Kinetics

The kinetics of the MB dye adsorption on the P@SiO_2 nanocomposite for various P@SiO_2 nanocomposite doses were tested in contact times ranging from 0.0 to 7.0 min, and the results obtained are illustrated in Figure 5a,b. The calculated kinetic parameters are summarized in Table 1. As shown in Table 1, the correlation coefficient (R^2) related to the pseudo-second-order is higher than that obtained for the pseudo-first-order. Moreover, the calculated maximum adsorption capacity for the pseudo-second-order matches well with the experimental data. This indicated that the adsorption kinetics of various P@SiO_2 nanocomposite doses were described very well with the pseudo-second-order. For this model, it is suggested that the rate-limiting step might be chemical adsorption for the adsorption of MB dye onto P@SiO_2 nanocomposite [23].

Table 1. The calculated parameters of the *pseudo*-first-order and *pseudo*-second-order kinetic model for various P@SiO_2 nano-composite.

Adsorbent Dose, mg	$q_{e\ exp}$ (mg/g)	First-Order Kinetic Parameter			Second-Order Kinetic Parameter		
		K_1 (min^{-1})	$q_{e\ cal}$ (mg/g)	R^2	K_2 (g mg^{-1} min^{-1})	$q_{e\ cal}$ (mg/g)	R^2
10	79.58	−0.31	21.38	0.981	0.069	80.00	0.996
15	58.67	−0.77	17.78	0.938	0.11	55.90	0.970
20	45.81	−0.54	8.79	0.927	0.26	46.10	0.999
25	37.9	−0.77	5.32	0.931	0.35	39.02	0.999

The mechanism and kinetics of the removal of MB dye onto P@SiO_2 nanocomposite nanoparticles were evaluated by applying the data obtained from the dye concentration experiment using the pseudo-first-order (Equation (S3)) and pseudo-second-order models (Equation (S5)). Moreover, the kinetic parameters obtained from the linear plots (Figure 5c,d) of the two models were calculated and recorded in Table 2. Referring to the values of R^2, the experimental data of the adsorption of MB dye on the P@SiO_2 nanocomposite showed a better fit with the pseudo-second-order models, which indicates that the dye species was chemically adsorbed and the adsorbent surface is the rate-limiting step [48].

Table 2. The calculated parameters of the pseudo-first-order and pseudo-second-order kinetic model for various concentrations of MB dye.

[MB], ppm	$q_{e\ exp}$ (mg/g)	First-Order Kinetic Parameter			Second-Order Kinetic Parameter		
		K_1 (min^{-1})	$q_{e\ cal}$ (mg/g)	R^2	K_2 (g mg^{-1} min^{-1})	$q_{e\ cal}$ (mg/g)	R^2
100	37.9	−0.77	5.32	0.899	0.36	38.46	0.999
150	50.85	−0.71	8.71	0.987	0.37	50.51	0.998
200	58.64	−1.14	18.88	0.988	0.24	59.17	0.998
300	73.95	−0.71	27.54	0.993	0.028	75.47	0.999

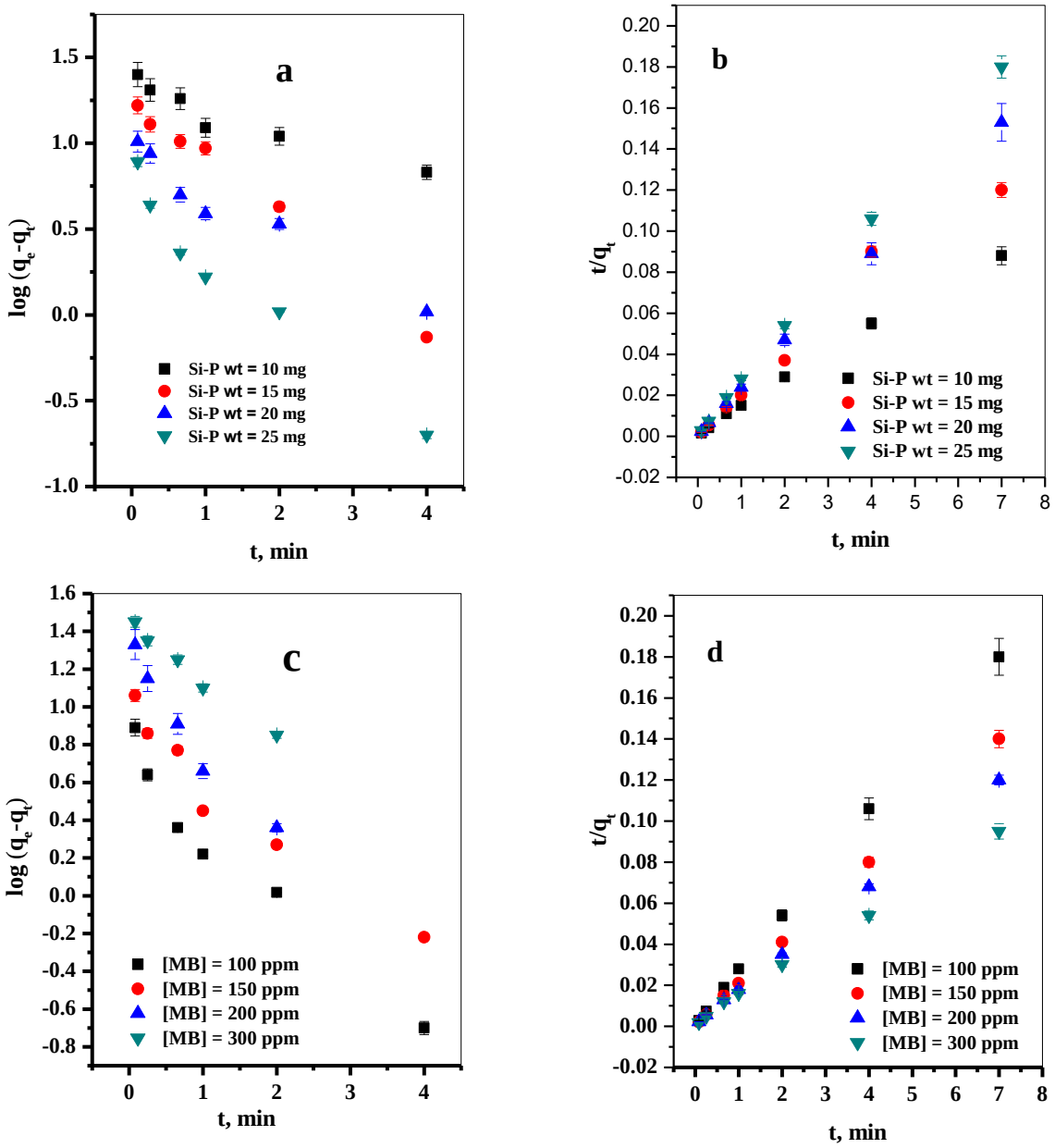


Figure 5. (**a**) Effect of contact time on removal percent of MB dye, (**b**) P@SiO_2 nanocomposite dose on equilibrium constant, (**c**) pseudo-first-order plot, (**d**) pseudo-second-order plot. ([P@SiO_2] = 10–25 mg/10 mL, [MB] = 100 ppm, pH = 7, T = 25 °C).

By plotting log (q_e–q_t) versus t at different pH values of the MB dye solution (Figure 6a,b), the correlation coefficient (R^2), the first-order rate constant (k_1), and q_e were calculated from the slopes and intercepts of the straight lines and listed in Table 3. Similarly, R^2, k_2, and q_e related to the pseudo-second-order were calculated from the linear plot of the t/q_t versus t at different pH values of the dye solution and recorded in Table 3. By comparing the values of R^2 related to the pseudo-first-order kinetic model with that in the case of the pseudo-second-order kinetic model, it can be observed that the R^2 in the pseudo-second-order kinetic model is higher than in the pseudo-first-order kinetic model. Moreover, the calculated q_e value obtained from the pseudo-second-order kinetic model is closer to the experimental q_e values. This indicates that the pseudo-second-order kinetic model best describes the adsorption kinetics rather than the pseudo-first-order model. To investigate the mechanism of the adsorption of MB dye at various temperatures, the Lagergren pseudo-first-order kinetic and pseudo-second-order kinetic models were applied (Figure 6c,d). The revealing parameters

of the two models were evaluated and summarized in Table 4. According to the data obtained, it can be decided that the pseudo-second-order equation is the better-fitting model. This is due to it owning higher R^2 values [48]. In addition, the calculated maximum adsorption capacities, q_e, from the pseudo-second-order model are close to the values of the experimental ones. This demonstrated that surface control mainly explains the adsorption processes rather than adsorbate diffusion. These results illustrated that chemical bonding or chemisorption between MB dye molecules and the active sites on the surface of P@SiO_2 nanocomposite might dominate the adsorption process, and this result agrees with what was reported in the literature [29].

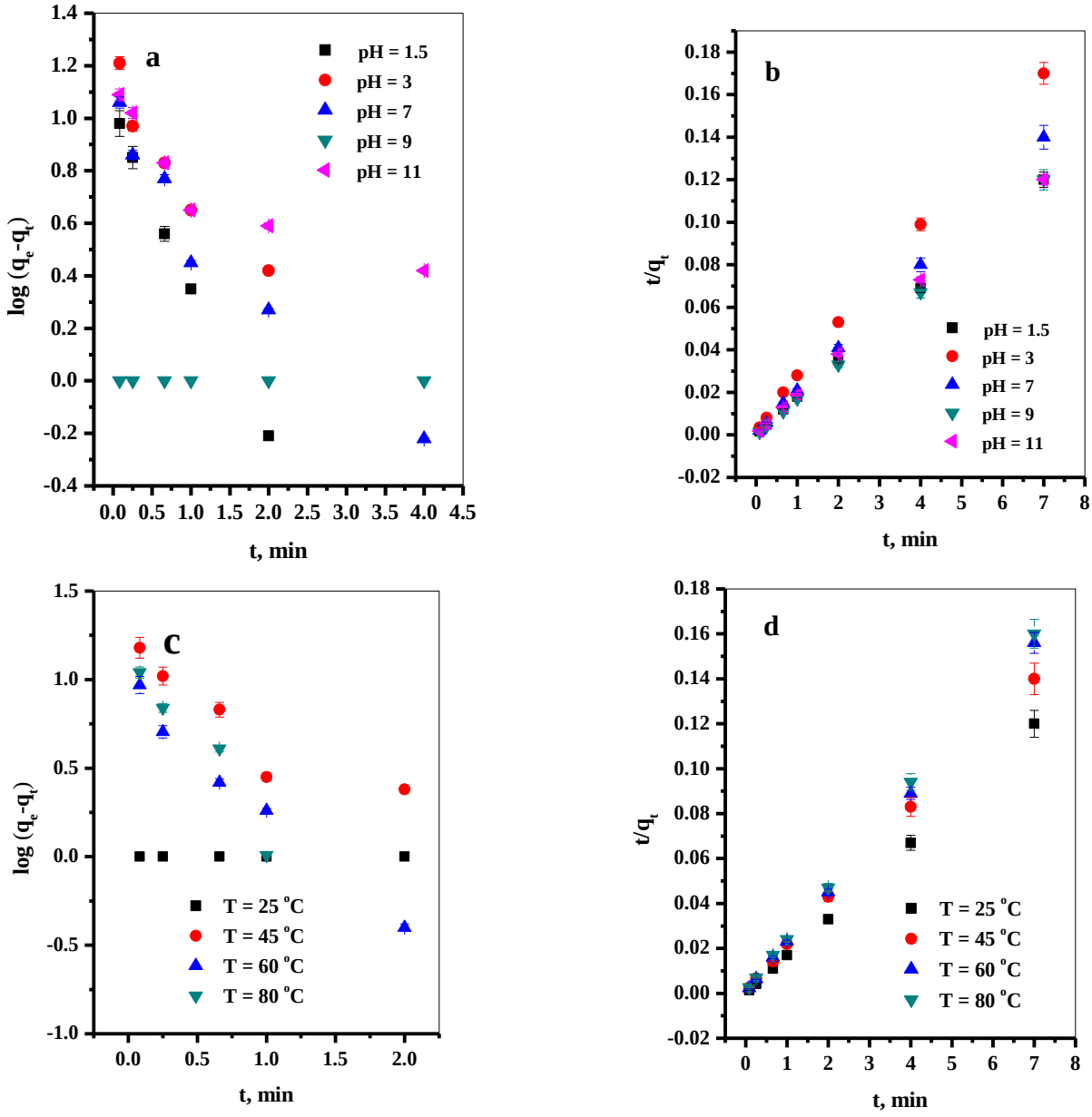


Figure 6. (**a**) Effect of contact time on removal percent of MB dye, (**b**) pH on the equilibrium constant, (**c**) pseudo-first-order plot, (**d**) pseudo-second-order plot (pH = 1.5–11, [MB] = 150 ppm, [P@SiO_2] = 25 mg/10 mL, T = 25 °C).

Table 3. The calculated parameters of the pseudo-first-order and pseudo-second-order kinetic model for various pH values.

pH	$q_{e\ exp}$ (mg/g)	Pseudo-First-Order Kinetic Parameter			Pseudo-Second-Order Kinetic Parameter		
		K_1 (min^{-1})	$q_{e\ cal}$ (mg/g)	R^2	K_2 (g mg^{-1} min^{-1})	$q_{e\ cal}$ (mg/g)	R^2
1.5	58.17	−1.45	9.95	0.94	0.43	58.48 ± 0.4	0.999
3	40.27	−0.88	13.12	0.886	0.17	41.67 ± 1.1	0.999
7	50.85	−0.71	8.17	0.927	0.36	50 ± 0.7	0.999
9	59.80	0.00	0.00	0.000	−1.34	58.48 ± 1.5	0.999
11	57.15	−0.37	9.55	0.64	0.16	58.14 ± 1.3	0.998

Table 4. The calculated parameters of the pseudo-first-order and pseudo-second-order kinetic model at different temperatures.

T, °C	$q_{e\ exp}$ (mg/g)	First-Order Kinetic Parameter			Second-Order Kinetic Parameter		
		K_1 (min^{-1})	$q_{e\ cal}$ (mg/g)	R^2	K_2 (g mg^{-1} min^{-1})	$q_{e\ cal}$ (mg/g)	R^2
25	59.80	0.00	0.00	0.000	−1.34	58.48 ± 0.5	0.999
45	48.41	−0.97	12.88	0.777	0.22	50 ± 0.8	0.999
60	44.74	−1.57	8.51	0.970	0.60	45.45 ± 0.3	0.999
80	42.51	−2.42	14.13	0.910	0.35	43.48 ± 0.6	0.999

3.2.6. Adsorption Isotherm

The most famous isotherms used to describe the adsorption isotherm are Langmuir, Freundlich, and Tempkin isotherm expressions given by Equations (S6)–(S8), respectively.

Langmuir isotherm supposes a monolayer of the adsorbate adsorbed on homogenously active sites with the same adsorption energies. Moreover, once these sites are occupied, no more adsorption takes place. Langmuir constants Q° and b (Table 5) can be obtained from the slope and intercept of the linear plot of C_e/q_e versus C_e as illustrated in Figure 7a.

Table 5. Calculated equilibrium constants for adsorption of MB.

Adsorbent	Langmuir Isotherm Model			Freundlich Isotherm Model			Tempkin Isotherm Model		
	Q° (mg/g)	b (L/mg)	R^2	n	K_f (mg/g)	R^2	B (J $mol^{-1)}$	A (L mg^{-1})	R^2
MB	76.92 ± 0.2	0.092	0.980	4.76	4.14	0.980	4.70	11.40	0.94

Dimensionless separation factor (R_L) for the MB dye adsorption onto the P@SiO_2 nanocomposite surface was determined from Equation (S6). If $R_L > 1$, unfavorable; $R_L = 1$, linear; $0 < R_L < 1$, favorable; $R_L = 0$, irreversible (Figure 7b). It can be observed that the R_L values between 0 and 1 indicate a favorable adsorption process.

The Freundlich isotherm suggested a heterogeneous surface with non-equivalent energetic binding sites. The Freundlich constants can be calculated by plotting ln q_e versus ln C_e (Figure 7c and Table 5). From the data in Table 5, $1/n < 1$, which suggests a normal Langmuir isotherm.

The adsorption performance of MB dye onto P@SiO_2 nanocomposite was assessed by referring to the Tempkin isotherm model (Equation (S8)), and the linear relationship is plotted in Figure 7d. The correlation coefficient ($R^2 = 0.940$) shows the poorest fit to the experimental adsorption equilibrium data, as summarized in Table 5.

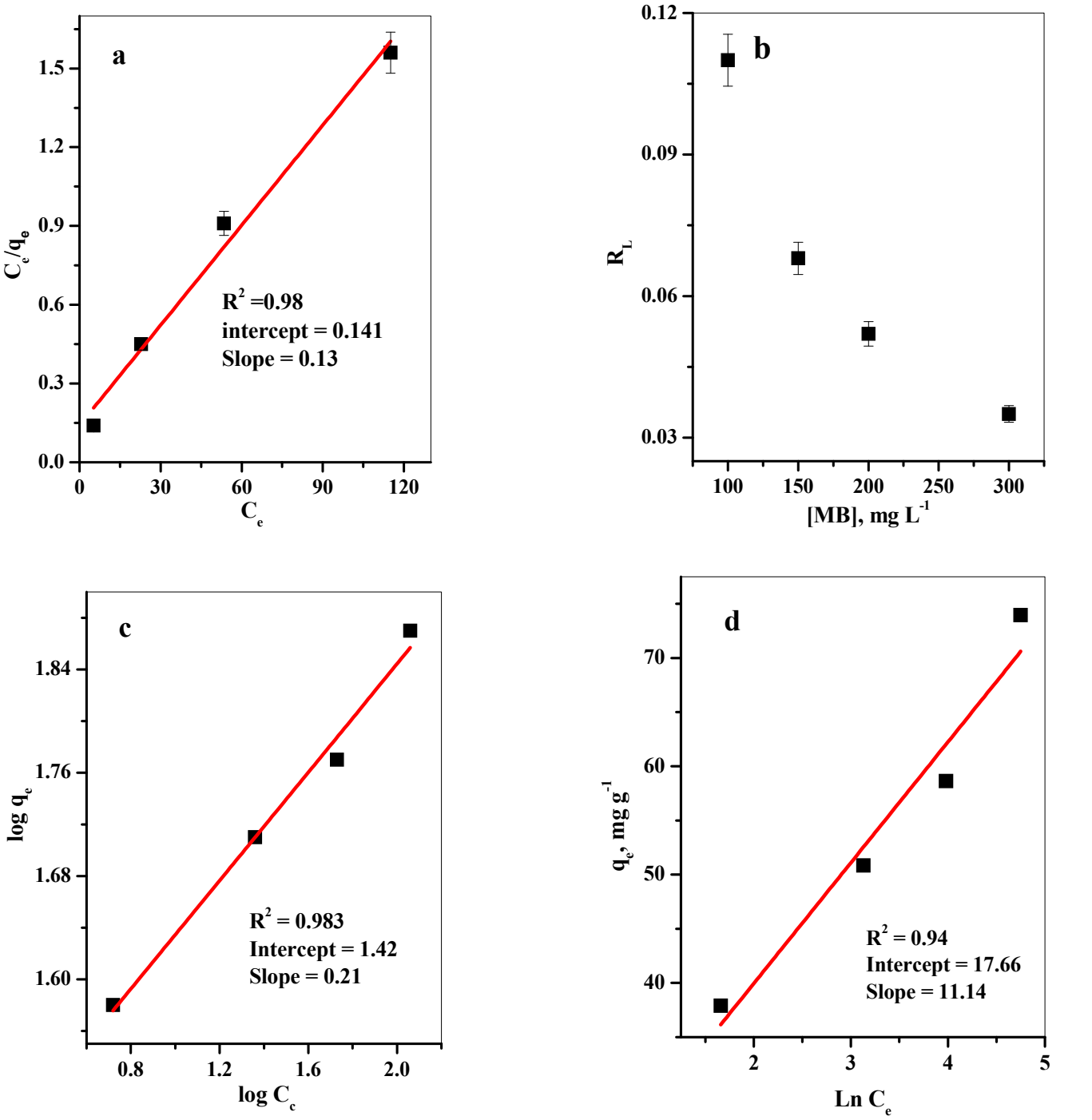


Figure 7. Adsorption isotherms: (**a**) Langmuir isotherm plot (**b**) Freundlich isotherm plot (**c**) R_L (**d**) Tempkin isotherm plot for removal of MB dye (t = 42. s, ([MB] = 100–300 ppm, [dose] = 25 mg/10 mL, pH = 7, T = 25 °C).

The obtained values of the correlation coefficient (R^2) (≈0.98) suggesting that the adsorption isotherm data of the adsorption of MB species onto P@SiO_2 nanocomposite fits better for both Langmuir and Freundlich isotherm models. Based on the closest values of the experimental and calculated Q_{max}, the adsorption results of MB species onto P@SiO_2 nanocomposite were fitted well with the Langmuir model representing monolayer adsorption on homogeneous surfaces [17,26]. Hence, the MB species sequestration processes occurred at P@SiO_2 nanocomposite surfaces via the monolayer adsorption systems [26,47].

3.2.7. Adsorption Thermodynamics

Thermodynamic parameters were determined from the linear plot of Ln K_c vis T^{-1} (Figure S4) and according to Equations (S8)–(S10) and summarized in Table 6. The negative ΔG° values make it clear that the adsorption of MB dye on P@SiO_2 nanocomposite is a spontaneous adsorption process. Moreover, the decrease showed for the ΔG° values with the increasing temperature from 298 to 353 K, demonstrating the adsorption performance is favored at lower temperatures and the adsorption of MB species onto P@SiO_2 nanocomposite is a spontaneous process [26,35]. The ΔH° had a negative value confirming the exothermic nature of the adsorption process. The negative value of ΔS° suggests decreasing in the randomness of the solid/solution interfaces [26]. Activation energies, Ea, lower than 42 kJ/mol, suggest a diffusion-controlled mechanism, and higher than that value exhibits chemisorptions behavior. Here, the calculated value of E_a is 45.3 kJ mol^{-1}; this indicates that the adsorption of MB onto P@SiO_2 nanocomposite is a chemically controlled process. The data represented in Figure 4b confirms this result. Also, the P@SiO_2 nanocomposite illustrates excellent efficiency in adsorbing MB dye molecules from both acidic and alkaline media. Therefore, we can conclude that the P@SiO_2 nanocomposite will not be regenerated well. This could be considered an advantage where the MB dye molecules will be restricted from release again into the surrounding environment after adsorption due to the chemical bonding or chemisorption between MB dye molecules and the active groups on the surface of the P@SiO_2 nanocomposite.

Table 6. Thermodynamic parameters for MB dye removal from aqueous media by P@SiO_2 nanocomposite.

	T (K)	MB
$-\Delta G$ (KJ mol^{-1})	298	1.982 ± 0.09
	318	1.356 ± 0.07
	333	0.435 ± 0.005
	353	−0.088 ± 0.001
$-\Delta H$ (KJ mol^{-1})	-	13.56 ± 0.3
$-\Delta S$ (KJ mol^{-1})		0.04 ± 0.008

3.2.8. Effect of Ionic Strength on the Adsorption Percent of MB Dye

In practical application, studying the effect of NaCl dose is very important to evaluate the influence of ionic strength on the adsorption percent of MB dye onto P@SiO_2 nanocomposite. Here, we study the effect of NaCl dose in the range 0.00–2.00 g on the removal percent of MB dye, as shown in Figure S5. It was observed that the NaCl dose did not affect the adsorption percent of MB dye in the studied range, as shown in Figures S5 and S6.

3.2.9. Adsorption Mechanism

The P@SiO_2 nanocomposite was prepared by combining sodium silicate and sodium phosphate. Hence, the binding sites, which were responsible for the interaction with the MB species, were mainly composed of silanol and phosphate groups. Upon contacting with the positive MB species pollutants in the aqueous media, the negative binding sites P@SiO_2 nanocomposite interact with the MB species through ionic bond and oxygen lone pair sharing. The proposed adsorption mechanism is illustrated in Figure 8. The electrostatic attractions between the positive MB species and the negative active sites of P@SiO_2

nanocomposite mainly depends on the reaction pH [49,50]. In an acidic environment, the H-atom will convert Si=O into Si-OH which will enhance the activity of these groups towards interaction with the positive MB species. On the other hand, as the pH of the media increases, the ionization of P-O^- Na^+ groups increase, which will increase the affinity of the P@SiO_2 nanocomposite towards the MB species. Also, the H-bonding becomes dominant in the adsorption mechanism and plays a vital role to improve the adsorption capacity [26,50]. P@SiO_2 nanocomposite and MB dye have many N-atoms; therefore, the adsorption capacities are enhanced due to the formation of N-H . . . N bonds between P@SiO_2 nanocomposite and MB species.

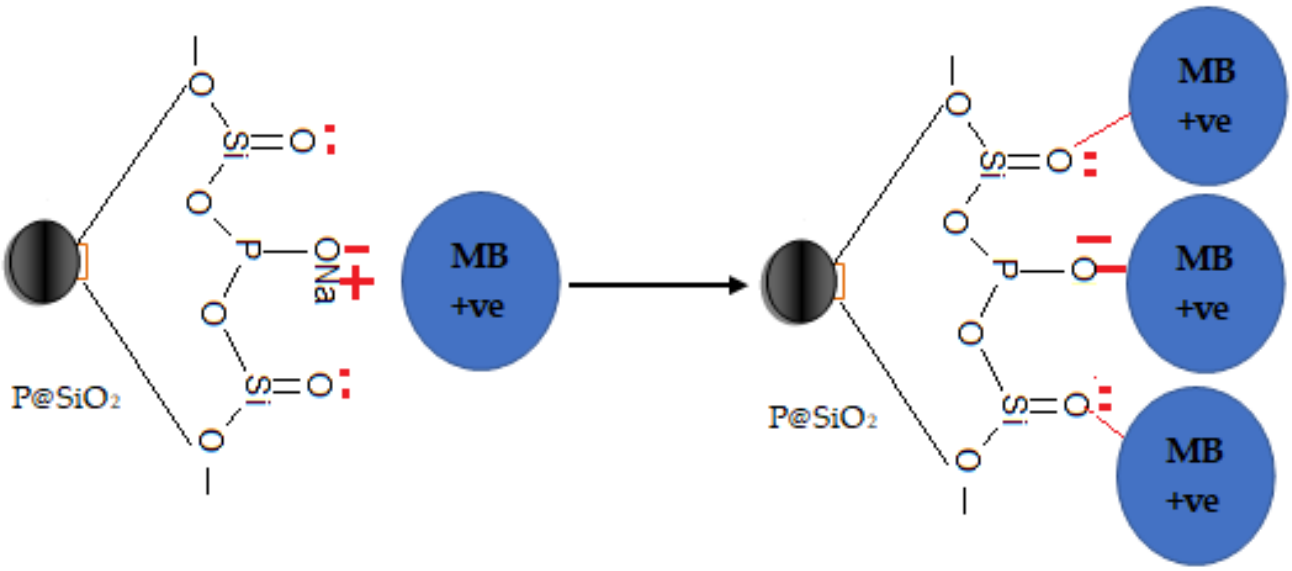


Figure 8. The proposed adsorption mechanism of MB dye onto P@SiO_2 nanocomposite from aqueous media.

3.3. Comparison Study

A comparative evaluation of the maximum adsorption capacity of P@SiO_2 nanocomposite to adsorb MB dye according to the Langmuir isotherm and other adsorbent materials in the literature is listed in Table 7 [49–79]. Referring to the recent literature, equilibrium time and adsorption capacities are the main goals for scientists to investigate and develop many novel adsorbent materials. Comparatively, the prepared P@SiO_2 nanocomposite illustrated considerable adsorption capacity compared to many novel materials and modified activated carbon materials. On the other hand, the obtained adsorption capacity of the prepared P@SiO_2 nanocomposite was lower than some reported adsorbents; the major advantages of the prepared adsorbent over those reported materials were the rapid adsorption rate and easy recovery from aqueous solution after the adsorption process for reuse. Also, for the prepared P@SiO_2 nanocomposite, the equilibrium time was reached rapidly within 100 s with an adsorption capacity of 76.9 mg/g. Therefore, the prepared P@SiO_2 nanocomposite is suggested as an available, high-potential, and promising sorbent nanocomposite to remove MB dye from an aqueous media with considerable efficiency. Also, the P@SiO_2 nanocomposite can meet commercial needs for water treatment applications.

Table 7. Comparison of the maximum adsorption capacities of P@SiO_2 with recently reported SiO_2-based materials to remove MB dye [49–79].

Adsorbent	T, min	Adsorbent dose	T, °C	pH	q_e, mg/g	Ref.
MOFs, MIL-101(Cr)	24 h	2.5 mg/10 mL	25	–	34.3	[49]
Fe_3O_4@SiO_2-CR	10	30 mg/30 mL	25	11	31.44	[50]
Mesoporous Fe_3O_4@SiO_2	5	1 mg/L	25	7	33.12	[51]
PLA-PEG/$MgSiO_3$ Membrane	–	3	25	10	79% [MB] = 5.5 ppm	[52]
Fe_3O_4@SiO_2-EDA-COOH	60	20 mg/50 mL	25	10	43.15	[53]
Monodispersed MSNs	6	5 mg/26 mL	25	7	34.23	[54]
(FA-DMSN)	6	10 mg/15 mL	25	7	90.7	[55]
CMMSNs	300	0.02 g/50 mL	25	7	43.03	[56]
SNFs-LMw	360	5 mg/10 mL	25	10	278.8	[57]
SNFs-HMw	240				123.3	
MSM@PDA	15	0.37 g	25	10	83.8	[58]
γ-Fe_2O_3/SiO_2	240	2 g/L	25	7	116.09	[59]
Fe_3O_4@Void@m.SiO_2	3	5 mg/15 mL	25	9	163.93	[60]
Fe_3O_4-graphene@mesoporous SiO_2 Nanocomposites	15	10	40	11	0.98–102.2	[61]
Silica Xerogel Synthesized from Volcanic Tuff	60	0.0016 g/mL	40	5	51.967	[62]
Silica gel derived from Algerian siliceous	240	1 g/L	25	6.3	80.45	[63]
Cysteine-Functionalized Mesoporous Silica ((MSN-Cys)	80	10 mg/10 mL	25	8.5	140	[64]
(MSN) (MSN-NH_2)	30	0.05 g/25 mL	–	11	2.899 1.736	[65]
βCD-SNHS	720	0.01 g/7 mL	27	10.5	60.55	[66]
Modified Nano-silica with Bismuth and Iron	20	8 g/L	25	5-6	9.54	[67]
Mesoporous Silicalite-1	240	0.10 wt%/50 mL	30		19.04	[68]
Silica Nanoparticles (SNPs)	60	0.3 g/L	30	7	31	[69]
Mesoporous Silica Spheres	20	15 mg/15 mL	30	5-7	60	[70]
AC-$MnFe_2O_4$	15	24 mg/L	30	4	77.74	[71]
Activated Charcoal from Ficus carica bast	90	0.5 g/100 mL	30	8	47.62	[72]
Activated Carbon	120	0.1 g/100 mL	30	8	72	[73]
AC1	45	2 g/L	25	9	28.65	[74]
AC2	120				17.57	
AC3	120				0.809	
BCC	60	0.1 g/20 mL	25	7	11.63	[75]
BCAC-10					12.71	
BCAC-20					16.85	
DMWTAC	30	200	20	8	53	[76]
CNZL Activated Carbon	80	100	50	–	14.493	[77]
GFSF	360	3 g/L	27	8	19.18	[78]
Carbon Nanoparticles (TPCNPs)	90	50 mg/120 mL	20	5	98	[79]
P@Si	100 s	25 mg/10 mL	25	7	76.92	This work

4. Conclusions and Future Perspectives

Here, we investigated a simple hydrothermal strategy to preparеP@SiO_2 nanocomposite to efficiently remove methylene blue dye from an aqueous solution. SEM, EDX, XRD, and FTIR techniques were employed to characterize the prepared nanomaterial. Various parameters that affected the adsorption process were investigated, such as preparing

$P@SiO_2$ nanocomposite dose, MB dye concentration, pH, temperature, and NaCl dose in the kinetic study. An increase in the adsorbent dose leads to minimizing the amount of dye adsorbed to one gram of the adsorbent. While the adsorption capacity of MB dye (qe) increases with a further increase in the initial dye concentration. On the other hand, the maximum adsorption capacities of the MB dye have varied according to the pH values. Moreover, increasing the dye solution temperature will lead to a decrease in the maximum adsorption capacity of the adsorbate. Finally, NaCl at various doses does not affect MB adsorption. From the analysis of the experimental results, the pseudo-second-order was an excellent fit for the obtained data. Moreover, according to Langmuir isotherm, the $P@SiO_2$ nanocomposite shows excellent saturation capacity (76.92 mg g^{-1}) which was suitable compared to other adsorbents in the literature. The thermodynamic studies showed that the adsorption process is preferred at low temperatures, exothermic, and ordered at the solid/solution interface. Also, the comparison study showed the promising properties and adsorption efficiency of $P@SiO_2$ nanocomposite compared with other adsorbent materials. Also, $P@SiO_2$ nanocomposite can be recommended as an eco-friendly absorbent material to purify wastewater from various cationic pollutants with significant efficiency in future works.

Supplementary Materials: The following supporting information can be downloaded at: https://www.mdpi.com/article/10.3390/ma16020514/s1. Figure S1: SEM images of as prepared Si-P nanoparticles; Figure S2: The relation between q_e vs. C_e at different (a) $P@SiO_2$ nano-composite doses and (b) initial MB concentrations; Figure S3: The color of MB-dye variation as a function of at time 5–420 s at different pH values; Figure S4: Thermodynamic plots for MB-dye removal from aqueous media by $P@SiO_2$ nano-composite; Figure S5: Effect of NaCl doses on removal percent of MB-dye onto $P@SiO_2$ nanocomposite. ([$P@SiO_2$] = 10–25 mg/10 mL, [MB] = 100 ppm, pH =7, T = 25 °C); Figure S6: Color variation as a function of NaCl doses at intervals 0–420 s. References [80,81] are cited in Supplementary file.

Author Contributions: Conceptualization, A.I.A.-E., A.A.N., A.A.A. and S.B.; methodology, A.I.A.-E. and I.M.A.; software, I.M.A., A.M.E.A.-R., H.M.A.S., A.A.N., H.M.A.S. and A.M.E.A.-R.; validation, M.A.A., W.A.A.A., I.M.A. and S.B.; formal analysis, H.M.A., A.M.E.A.-R. and H.M.A.S.; investigation, H.M.A., W.A.A.A. and A.I.A.-E.; writing—original draft preparation, A.I.A.-E., M.A.A., W.A.A.A., I.M.A. and A.A.A.; writing—review and editing, A.I.A.-E., A.A.A., A.A.N. and S.B.; project administration, A.A.N.; funding acquisition, A.A.N. All authors have read and agreed to the published version of the manuscript.

Funding: This work was funded by the Deanship of Scientific Research at Jouf University under grant No. (DSR2022-RG-0130).

Institutional Review Board Statement: Not applicable.

Informed Consent Statement: Not applicable.

Data Availability Statement: Data is contained within the article.

Acknowledgments: This work was funded by the Deanship of Scientific Research at Jouf University under grant No. (DSR2022-RG-0130). The authors acknowledge support from the KIT-Publication Fund of the Karlsruhe Institute of Technology. Stefan Bräse is grateful for support from the DFG-funded cluster program "3D Matter Made To Order" under Germany's Excellence Strategy-2082/1-390761711. The authors acknowledge grants from the Science and Technology Commission of Shanghai Municipality (19440741300).

Conflicts of Interest: The authors declare no conflict of interest.

References

1. Yaqoob, A.A.; Parveen, T.; Umar, K.; Mohamad Ibrahim, M.N. Role of Nanomaterials in the Treatment of Wastewater: A Review. *Water* **2020**, *12*, 495. [CrossRef]
2. Sarkar, N.; Sahoo, G.; Swain, S.K. Reduced graphene oxide decorated superporous polyacrylamide based interpenetrating network hydrogel as dye adsorbent. *Mater. Chem. Phys.* **2020**, *250*, 123022. [CrossRef]

3. Yaqoob, A.A.; Ahmad, H.; Parveen, T.; Ahmad, A.; Oves, M.; Ismail, I.M.I.; Qari, H.A.; Umar, K.; Mohamad Ibrahim, M.N. Recent Advances in Metal Decorated Nanomaterials and Their Various Biological Applications: A Review. *Front. Chem.* **2020**, *8*, 341. [CrossRef] [PubMed]
4. Ahmad, A.; Mohd-Setapar, S.H.; Chuong, C.S.; Khatoon, A.; Wani, W.A.; Kumard, R.; Rafatullah, M. Recent advances in new generation dye removal technologies: Novel search for approaches to reprocess wastewater. *RSC Adv.* **2015**, *5*, 30801–30818. [CrossRef]
5. Salama, A.; Abou-Zeid, R.E. Ionic chitosan/silica nanocomposite as efficient adsorbent for organic dyes. *Intern. J. Biol. Macromol.* **2021**, *188*, 404–410. [CrossRef]
6. Jiao, Y.; Wan, C.; Bao, W.; Gao, H.; Liang, D.; Li, J. Facile hydrothermal synthesis of Fe_3O_4@cellulose aerogel nanocomposite and its application in Fenton-like degradation of Rhodamine. *B. Carbohydr. Polym.* **2018**, *189*, 371–378. [CrossRef]
7. Abou-Zeid, R.E.; Khiari, R.; El-Wakil, N.; Dufresne, A. Current state and new trends in the use of cellulose nanomaterials for wastewater treatment. *Biomacromolecules* **2019**, *20*, 573–597. [CrossRef]
8. Kong, X.-P.; Zhang, B.-H.; Wang, J. Multiple Roles of Mesoporous Silica in Safe Pesticide Application by Nanotechnology: A Review. *J. Agric. Food Chem.* **2021**, *69*, 6735–6754. [CrossRef]
9. Khabra, A.; Cohen, H.; Pinhasi, G.A.; Querol, X.; Córdoba Sola, P.; Zidki, T. Synthesis of a $SiO_2/Co(OH)_2$ Nanocomposite Catalyst for SO_X/NO_X Oxidation in Flue Gas. *Catalysts* **2023**, *13*, 29. [CrossRef]
10. Huang, X.; Li, L.; Zhao, S.; Zhao, S.; Tong, L.; Li, Z.; Peng, Z.; Lin, R.; Zhou, L.; Peng, C.; et al. MOF-Like 3D Graphene-Based Catalytic Membrane Fabricated by One-Step Laser Scribing for Robust Water Purification and Green Energy Production. *Nano-Micro Lett.* **2022**, *14*, 174. [CrossRef]
11. Oyekanmi, A.A.; Latiff, A.A.A.; Daud, Z.; Mohamed, R.M.S.R.; Ismail, N.; Aziz, A.A.; Rafatullah, M.; Hossain, K.; Ahmad, A.; Abiodun, A.K. Adsorption of cadmium and lead from palm oil mill effluent using bone-composite: Optimisation and isotherm studies. *Int. J. Environ. Anal. Chem.* **2019**, *99*, 707–725. [CrossRef]
12. Idris, M.O.; Yaqoob, A.A.; Ibrahim, M.N.M.; Ahmad, A.; Alshammari, M.B. Introduction of Adsorption Techniques for Heavy Metals Remediation. In *Emerging Techniques for Treatment of Toxic Metals from Wastewater*; Elsevier: Amsterdam, The Netherlands, 2023; pp. 1–18. [CrossRef]
13. Hao, Y.; Cui, Y.; Peng, J.; Zhao, N.; Li, S.; Zhai, M. Preparation of graphene oxide/ cellulose composites in ionic liquid for Ce (III) removal. *Carbohydr. Polym.* **2019**, *208*, 269–275. [CrossRef] [PubMed]
14. Xie, L.-Q.; Jiang, X.-Y.; Yu, J.-G. A Novel Low-Cost Bio-Sorbent Prepared from Crisp Persimmon Peel by Low-Temperature Pyrolysis for Adsorption of Organic Dyes. *Molecules* **2022**, *27*, 5160. [CrossRef]
15. Birniwa, A.H.; Mahmud, H.N.M.E.; Abdullahi, S.S.; Habibu, S.; Jagaba, A.H.; Ibrahim, M.N.M.; Ahmad, A.; Alshammari, M.B.; Parveen, T.; Umar, K. Adsorption Behavior of Methylene Blue Cationic Dye in Aqueous Solution Using Polypyrrole-Polyethylenimine Nano-Adsorbent. *Polymers* **2022**, *14*, 3362. [CrossRef] [PubMed]
16. Bangari, R.S.; AnshulYadav, A.; Awasthi, P.; Sinha, N. Experimental and theoretical analysis of simultaneous removal of methylene blue and tetracycline using boron nitride nanosheets as adsorbent. *Colloids Surf. A Physicochem. Eng. Asp.* **2022**, *634*, 127943. [CrossRef]
17. Tran, T.K.N.; Phan, C.P.K.; Ngo, T.C.Q.; Hoang, N.B.; Truong, L.D.; Nguyen, T.K.O. Synthesis and Characterization Bimetallic Organic Framework CoxFex(BDC) and Adsorption Cationic and Anionic Dyes. *Processes* **2022**, *10*, 1352. [CrossRef]
18. Bazan-Wozniak, A.; Wolski, R.; Paluch, D.; Nowicki, P.; Pietrzak, R. Removal of Organic Dyes from Aqueous Solutions by Activated Carbons Prepared from Residue of Supercritical Extraction of Marigold. *Materials* **2022**, *15*, 3655. [CrossRef]
19. Sarojini, G.; Babub, S.V.; Rajamohan, N.; Rajasimm, M.; Pugazhendhi, A. Optimization, Application of a polymer-magnetic-algae based nanocomposite for the removal of methylene blue—Characterization, parametric and kinetic studies. *Environ. Pollut.* **2022**, *292*, 118376. [CrossRef]
20. Gao, J.; Li, Z.; Wang, Z.; Chen, T.; Hu, G.; Zhao, Y.; Han, X. Facile Synthesis of Sustainable Tannin/Sodium Alginate Composite Hydrogel Beads for Efficient Removal of Methylene Blue. *Gels* **2022**, *8*, 486. [CrossRef]
21. Ihaddaden, S.; Aberkane, D.; Boukerroui, A.; Robert, D. Removal of methylene blue (basic dye) by coagulation-flocculation with biomaterials (bentonite and Opuntia ficus indica). *J. Water Proc. Eng.* **2022**, *49*, 102952. [CrossRef]
22. Dadashi, J.; Khaleghian, M.; Mirtamizdoust, B.; Hanifehpour, Y.; Joo, S.W. Fabrication of Copper(II)-Coated Magnetic Core-Shell Nanoparticles Fe3O4@SiO2: An Effective and Recoverable Catalyst for Reduction/Degradation of Environmental Pollutants. *Crystals* **2022**, *12*, 862. [CrossRef]
23. Chen, T.; Liu, H.; Gao, J.; Hu, G.; Zhao, Y.; Tang, X.; Han, X. Efficient Removal of Methylene Blue by Bio-Based Sodium Alginate/Lignin Composite Hydrogel Beads. *Polymers* **2022**, *14*, 2917. [CrossRef] [PubMed]
24. Zango, Z.U.; Dennis, J.O.; Aljameel, A.I.; Usman, F.; Ali, M.K.M.; Abdulkadir, B.A.; Algessair, S.; Aldaghri, O.A.; Ibnaouf, K.H. Effective Removal of Methylene Blue from SimulatedWastewater Using ZnO-Chitosan Nanocomposites: Optimization, Kinetics, and Isotherm Studies. *Molecules* **2022**, *27*, 4746. [CrossRef] [PubMed]
25. Bhatti, M.A.; Gilani, S.J.; Shah, A.A.; Channa, I.A.; Almani, K.F.; Chandio, A.D.; Halepoto, I.A.; Tahira, A.; Bin Jumah, M.N.; Ibupoto, Z.H. Effective Removal of Methylene Blue by Surface Alteration of TiO_2 with Ficus Carica Leaf Extract under Visible Light. *Nanomaterials* **2022**, *12*, 2766. [CrossRef]
26. Alshahrani, A.A.; Alorabi, A.Q.; Hassan, M.S.; Amna, T.; Azizi, M. Chitosan-Functionalized Hydroxyapatite-Cerium Oxide Heterostructure: An Efficient Adsorbent for Dyes Removal and Antimicrobial Agent. *Nanomaterials* **2022**, *12*, 2713. [CrossRef]

27. Blaga, A.C.; Tanasa, A.M.; Cimpoesu, R.; Tataru-Farmus, R.-E.; Suteu, D. Biosorbents Based on Biopolymers from Natural Sources and FoodWaste to Retain the Methylene Blue Dye from the Aqueous Medium. *Polymers* **2022**, *14*, 2728. [CrossRef]
28. Yaqoob, A.A.; Ibrahim, M.N.M.; Reddy, A.V.B. Toxicology and Environmental Application of Carbon Nanocomposite. In *Environmental Remediation through Carbon Based Nano Composites*; Springer: Berlin/Heidelberg, Germany, 2021; pp. 1–18. [CrossRef]
29. Wang, F.; Zhang, J.; Jia, D.M. Facile synthesis of shell-core structured Fe_3O_4@ACS as recyclable magnetic adsorbent for methylene blue removal. *J. Dispers. Sci. Technol.* **2019**, *40*, 1736–1743. [CrossRef]
30. Bounaas, M.; Bouguettoucha, A.; Chebli, D.; Gatica, J.M.; Vidal, H. Role of the Wild Carob as Biosorbent and as Precursor of a New High-Surface-Area Activated Carbon for the Adsorption of Methylene Blue. *Arab. J. Sci. Eng.* **2021**, *46*, 325–341. [CrossRef]
31. Venkatesan, R.; Alagumalai, K.; Raorane, C.J.; Raj, V.; Shastri, D.; Kim, S.-C. Morphological, Mechanical, and Antimicrobial Properties of PBAT/Poly (Methyl Methacrylate-*co*-Maleic Anhydride)–SiO_2 Composite Films for Food Packaging Applications. *Polymers* **2023**, *15*, 101. [CrossRef]
32. Sharma, P.; Prakash, J.; Kaushal, R. An insight into the green synthesis of SiO_2 nanostructures as a novel adsorbent for removal of toxic water pollutants. *Environ. Res.* **2022**, *212*, 113328. [CrossRef]
33. Beagan, A.; Alotaibi, K.; Almakhlafi, M.; Algarabli, W.; Alajmi, N.; Alanazi, M.; Alwaalah, H.; Alharbi, F.; Alshammari, R.; Alswieleh, A. Amine and sulfonic acid functionalized mesoporous silica as an effective adsorbent for removal of methylene blue from contaminated water. *J. King SaudUniv. Sci.* **2022**, *34*, 101762. [CrossRef]
34. Jadhav, S.A.; Garud, H.B.; Patil, A.H.; Patil, G.D.; Patil, C.R.; Dongale, T.D.; Patil, P.S. Recent advancements in silica nanoparticles based technologies for removal of dyes from water. *Colloid Interface Sci. Commun.* **2019**, *30*, 100181. [CrossRef]
35. Li, Y.; Wang, S.; Shen, Z.; Li, X.; Zhou, Q.; Sun, Y.; Wang, T.; Liu, Y.; Gao, Q. Gradient Adsorption of Methylene Blue and Crystal Violet onto Compound Microporous Silica from Aqueous Medium. *ACS Omega* **2020**, *5*, 43–28382. [CrossRef] [PubMed]
36. Jesionowski, T.; Krysztafkiewicz, A. Preparation of the hydrophilic/hydrophobic silica particles. *Colloids Surf. A Physicochem. Eng. Asp.* **2002**, *207*, 49–58. [CrossRef]
37. Lee, M.S.; Jo, N.J. Coating of methyltriethoxysilane-modified colloidal silica on polymer substrates for abrasion resistance. *J. Sol-Gel Sci. Technol.* **2002**, *24*, 175–180. [CrossRef]
38. Hah, H.J.; Koo, S.M. Surface modification of PTMS particles with organosilanes: TEOS-, VTMS-, and MTMS-modified par-524 ticles. *J. Sol-Gel Sci. Technol.* **2004**, *31*, 117–121. [CrossRef]
39. Alswieleh, A.M. Modification of Mesoporous Silica Surface by Immobilization of Functional Groups for Controlled Drug Release. *J. Chem.* **2020**, *2020*, 9176257. [CrossRef]
40. Mary, K.A.A.; Unnikrishnan, N.V.; Philip, R. Cubic to amorphous transformation of Se in silica with improved ultrafast optical nonlinearity. *RSC Adv.* **2015**, *5*, 14034. [CrossRef]
41. Sanosh, K.P.; Chu, M.C.; Balakrishnan, A.; Kim, T.N.; Cho, S.J. Preparation and characterization of nano-hydroxyapatite powder using sol-gel technique. *Bull Mater. Sci.* **2009**, *32*, 465–470. [CrossRef]
42. Seifzadeh, D.; Hollagh, A.R. Corrosion Resistance Enhancement of AZ91D Magnesium Alloy by Electroless Ni-Co-P Coating and Ni-Co-P-SiO_2 Nanocomposite. *JMEPEG* **2014**, *23*, 4109–4121. [CrossRef]
43. Munir, M.; Nazar, M.F.; Zafar, M.N.; Zubair, M.; Ashfaq, M.; Hosseini-Bandegharaei, A.; Khan, S.U.-D.; Ahmad, A. Effective Adsorptive Removal of Methylene Blue from Water by Didodecyldimethylammonium Bromide-Modified Brown Clay. *ACS Omega* **2020**, *5*, 16711–16721. [CrossRef] [PubMed]
44. Martis, L.J.; Parushuram, N.; Sangappa, Y. Preparation, characterization, and methylene blue dye adsorption study of silk fibroin–graphene oxide nanocomposites. *Environ. Sci. Adv.* **2022**, *1*, 285. [CrossRef]
45. Gorzin, F.; Bahri Rasht Abadi, M.M. Adsorption of Cr(VI) from aqueous solution by adsorbent prepared from paper mill sludge: Kinetics and thermodynamics studies. *Adsorpt. Sci. Technol.* **2018**, *36*, 149–169. [CrossRef]
46. Yagub, M.T.; Sen, T.K.; Ang, M. Removal of cationic dye methylene blue (MB) from aqueous solution by ground raw and base modified pine cone powder. *Environ. Earth Sci.* **2014**, *71*, 1507–1519. [CrossRef]
47. Zhu, Y.; Yi, B.; Yuan, Q.; Wu, Y.; Wang, M.; Yan, S. Removal of methylene blue from aqueous solution by cattle manure-derived low temperature biochar. *RSC Adv.* **2018**, *8*, 19917. [CrossRef]
48. Ramutshatsha-Makhwedzha, D.; Mavhungu, A.; Moropeng, M.L.; Mbaya, R. Activated carbon derived from waste orange and lemon peels for the adsorption of methyl orange and methylene blue dyes from wastewater. *Heliyon* **2022**, *8*, e09930. [CrossRef]
49. Zou, M.; Zhu, H.; Dong, M.; Zhao, T. Template Method for Synthesizing Hierarchically Porous MIL-101(Cr) for Efficient Removal of Large Molecular Dye. *Materials* **2022**, *15*, 5763. [CrossRef]
50. Yimin, D.; Jiaqi, Z.; Danyang, L.; Lanli, N.; Liling, Z.; Yi, Z.; Xiaohong, Z. Preparation of Congo Red Functionalized Fe_3O_4@SiO_2 Nanoparticle and Its Application for the Removal of Methylene Blue. Colloids Surf. *A Physicochem. Eng. Asp.* **2018**, *550*, 90–98. [CrossRef]
51. Tan, X.; Lu, L.; Wang, L.; Zhang, J. Facile Synthesis of Bimodal Mesoporous Fe_3O_4@SiO_2 Composite for Efficient Removal of Methylene Blue. *Eur. J. Inorg. Chem.* **2015**, *2015*, 2928–2933. [CrossRef]
52. Hasanuddin, N.I.; Mokhtar, W.N.A.W.; Othaman, R.; Anuar, F.H. Poly(lactic acid)-poly(ethylene glycol)/Magnesium Silicate Membrane for Methylene Blue Removal: Adsorption Behavior, Mechanism, Ionic Strength and Reusability Studies. *Membranes* **2022**, *12*, 198. [CrossRef]
53. Jiaqi, Z.; Yimin, D.; Danyang, L.; Shengyun, W.; Liling, Z.; Yi, Z. Synthesis of Carboxyl-Functionalized Magnetic Nanoparticle for the Removal of Methylene Blue. Colloids Surf. *A Physicochem. Eng. Asp.* **2019**, *572*, 58–66. [CrossRef]

54. Qin, P.; Yang, Y.; Zhang, X.; Niu, J.; Yang, H.; Tian, S.; Zhu, J.; Lu, M. Highly Efficient, Rapid, and Simultaneous Removal of Cationic Dyes from Aqueous Solution Using Monodispersed Mesoporous Silica Nanoparticles as the Adsorbent. *Nanomaterials* **2018**, *8*, 4. [CrossRef] [PubMed]
55. Almethen, A.A.; Alotaibi, K.M.; Alhumud, H.S.; Alswieleh, A.M. Highly Efficient and Rapid Removal of Methylene Blue from Aqueous Solution Using Folic Acid-Conjugated Dendritic Mesoporous Silica Nanoparticles. *Processes* **2022**, *10*, 705. [CrossRef]
56. Li, Y.; Zhou, Y.; Nie, W.; Song, L.; Chen, P. Highly Efficient Methylene Blue Dyes Removal from Aqueous Systems by Chitosan Coated Magnetic Mesoporous Silica Nanoparticles. *J. Porous Mater.* **2015**, *22*, 1383–1392. [CrossRef]
57. Farias, R.M.C.; Severo, L.L.; Klamczynski, A.P.; Medeiros, E.S.; Santana, L.N.L.; Neves, G.A.; Glenn, G.M.; Menezes, R.R. Solution Blow Spun Silica Nanofibers: Influence of Polymeric Additives on the Physical Properties and Dye Adsorption Capacity. *Nanomaterials* **2021**, *11*, 3135. [CrossRef] [PubMed]
58. Germi, T.A.; Nematollahzadeh, A. Bimodal porous silica microspheres decorated with polydopamine nanoparticles for the adsorption of methylene blue in fixed-bed columns. *J. Colloid Interface Sci.* **2016**, *470*, 172–182. [CrossRef] [PubMed]
59. Chen, D.; Zeng, Z.; Zeng, Y.; Zhang, F.; Wang, M. Removal of methylene blue and mechanism on magnetic -Fe_2O_3/SiO_2 nanocomposite from aqueous solution. *Water Resour. Ind.* **2016**, *15*, 1–13. [CrossRef]
60. Mirbagheri, R.; Elhamifar, D.; Shaker, M. Yolk–shell structured magnetic mesoporous silica: A novel and highly efficient adsorbent for removal of methylene blue. *Sci. Rep.* **2021**, *11*, 23259. [CrossRef]
61. Wu, X.-L.; Shi, Y.; Zhong, S.; Lin, H.; Chen, J.-R. Facile synthesis of Fe_3O_4- graphene@ mesoporous SiO_2 nanocomposites for efficient removal of Methylene Blue. *Appl. Surf. Sci.* **2016**, *378*, 80–86. [CrossRef]
62. Kaya, G.G.; Yilmaz, E.; Deveci, H. A novel silica xerogel synthesized from volcanic tuff as an adsorbent for high-efficient removal of methylene blue: Parameter optimization using Taguchi experimental design. *J. Technol. Biotechnol.* **2019**, *94*, 2729–2737. [CrossRef]
63. Ingrachen-Brahmi, D.; Belkacemi, H.; Ait Brahem-Mahtout, L. Adsorption of Methylene Blue on silica gel derived from Algerian siliceous by-product of kaolin. *J. Mater. Environ. Sci.* **2020**, *11*, 1044–1057.
64. Beagan, A.M. Investigating Methylene Blue Removal from Aqueous Solution by Cysteine-Functionalized Mesoporous Silica. *J. Chem.* **2021**, *2021*, 8839864. [CrossRef]
65. Chueachota, R.; Wongkhueng, S.; Khankam, K.; Lakrathok, T.; Kaewnon, A.; Naowanon, W.; Amnuaypanich, S.; Nakhowong, R. Adsorption efficiency of methylene blue from aqueous solution with amine-functionalized mesoporous silica nanospheres by co-condensation biphasic synthesis: Adsorption condition and equilibrium studies. *Mater. Today Proc.* **2018**, *5*, 14079–14085. [CrossRef]
66. Ebadi, A.; Rafati. A.A. Preparation of silica mesoporous nanoparticles functionalized with β-cyclodextrin and its application for methylene blue removal. *J. Mol. Liq.* **2015**, *209*, 239–245. [CrossRef]
67. Salimi, F.; Tahmasobi, K.; Karami, C.; Jahangiri, A. Preparation of Modified nano-SiO_2 by Bismuth and Iron as a novel Remover of Methylene Blue from Water Solution. *J. Mex. Chem. Soc.* **2017**, *61*, 250–259. [CrossRef]
68. Radoor, S.; Karayil, J.; Jayakumar, A.; Parameswaranpillai, J.; Siengchin, S. Release of toxic methylene blue from water by mesoporous silicalite-1: Characterization, kinetics and isotherm studies. *Appl. Water Sci.* **2021**, *11*, 110. [CrossRef]
69. Esa, Y.A.M.; Sapawe, N. Removal of methylene blue from aqueous solution using silica nanoparticle extracted from skewer coconut leaves. *Mater. Today Proc.* **2020**, *31*, 398–401. [CrossRef]
70. de Paula, F.D.C.; Effting, L.; Arízaga, G.G.C.; Giona, R.M.; Tessaro, A.L.; Bezerra, F.M.; Bail, A. Spherical mesoporous silica designed for the removal of methylene blue from water under strong acidic conditions. *Environ. Technol.* **2022**, *43*, 2278–2289. [CrossRef]
71. Adeogun, A.I. Removal of methylene blue dye from aqueous solution using activated charcoal modified manganese ferrite (AC-$MnFe_2O_4$): Kinetics, isotherms, and thermodynamics studies. *Part. Sci. Technol.* **2020**, *38*, 756–767. [CrossRef]
72. Pathania, D.; Sharma, S.; Singh, P. Removal of methylene blue by adsorption onto activated carbon developed from Ficus carica bast. *Arab. J. Chem.* **2017**, *10*, S1445–S1451. [CrossRef]
73. Baytar, O.; Ceyhan, A.A.; Şahin, Ö. Production of activated carbon from Elaeagnus angustifolia seeds using H_3PO_4 activator and methylene blue and malachite green adsorption. *Int. J. Phytoremediation* **2021**, *23*, 693–703. [CrossRef] [PubMed]
74. El-Sayed, G.O.; Yehia, M.M.; Asaad, A.A. Assessment of activated carbon prepared from corncob by chemical activation with phosphoric acid. *Water Resour. Ind.* **2014**, *7*, 66–75. [CrossRef]
75. Thabede, P.M.; Shooto, N.D.; Naidoo, E.B. Removal of methylene blue dye and lead ions from aqueous solution using activated carbon from black cumin seeds. *S. Afr. J. Chem. Eng.* **2020**, *33*, 39–50. [CrossRef]
76. Kassahun, E.; Mekuria, S.; Beyan, S.M. Specific Surface Area Enhancement of Waste Tire-Based Activated Carbon by Demineralization Technique and Adsorption of Methylene Blue. *Int. J. Chem. Eng.* **2022**, *2022*, 8198551. [CrossRef]
77. IbrahimTouzani, I.; Fikri-Benbrahim, K.; Ahlafi, H.; Ihssane, B.; Boudouch, O. Characterization of Ziziphus lotus' Activated Carbon and Evaluation of Its Adsorption Potential. *J. Environ. Public Health* **2022**, *2022*, 8502211. [CrossRef]
78. Zhang, Y.; Wang, R.; Qiu, G.; Jia, W.; Guo, Y.; Guo, F.; Wu, J. Synthesis of Porous Material from Coal Gasification Fine Slag Residual Carbon and Its Application in Removal of Methylene Blue. *Molecules* **2021**, *26*, 6116. [CrossRef]
79. Abdulkhair, B.Y.; Elamin, M.R. Low-Cost Carbon Nanoparticles for Removing Hazardous Organic Pollutants from Water: Complete Remediation Study and Multi-Use Investigation. *Inorganics* **2022**, *10*, 136. [CrossRef]

80. Lagergren, S. About the Theory of So-Called Adsorption of Soluble Substances. *K. Sven. Vetenskapsakademiens. Handl. Band* **1898**, *24*, 527.
81. Ho, Y.S.; McKay, G. The sorption of lead (II) ions on peat. *Water Res.* **1999**, *33*, 578–584. [CrossRef]

Disclaimer/Publisher's Note: The statements, opinions and data contained in all publications are solely those of the individual author(s) and contributor(s) and not of MDPI and/or the editor(s). MDPI and/or the editor(s) disclaim responsibility for any injury to people or property resulting from any ideas, methods, instructions or products referred to in the content.